Pis'ma v ZhETF, vol. 96, iss. 12, pp. 870 – 874

New topological surface state in layered topological insulators: unoccupied Dirac cone

S. V. Eremeev[+*1)], *I. V. Silkin*[*], *T. V. Menshchikova*[*], *A. P. Protogenov*[×], *E. V. Chulkov*[°▽]

[+] *Institute of Strength Physics and Materials Science of the SB of the RAS, 634021 Tomsk, Russia*

[*] *Tomsk State University, 634050 Tomsk, Russia*

[×] *Institute of Applied Physics of the RAS, 603950 N.Novgorod, Russia*

[°] *Donostia International Physics Center, 20018 San Sebastián, Basque Country, Spain*

[▽] *Departamento de Física de Materiales UPV/EHU and Centro de Física de Materiales CFM and Centro Mixto CSIC-UPV/EHU, 20080 San Sebastián/Donostia, Basque Country, Spain*

Submitted 30 October 2012

The unoccupied states in topological insulators Bi_2Se_3, $PbSb_2Te_4$, and $Pb_2Bi_2Te_2S_3$ are studied by the density functional theory methods. It is shown that a surface state with linear dispersion emerges in the inverted conduction band energy gap at the center of the surface Brillouin zone on the (0001) surface of these insulators. The alternative expression of $\mathbb{Z}_2$ invariant allowed us to show that a necessary condition for the existence of the second $\bar{\Gamma}$ Dirac cone is the presence of local gaps at the time reversal invariant momentum points of the bulk spectrum and change of parity in one of these points.

Three-dimensional topological insulators (TIs) are characterized by presence of the topological surface state (SS) emergence in the principal band gap [1]. This spin-polarized linearly dispersing surface state forming Dirac cone arises from a symmetry inversion of the bulk bands at band gap edges owing to the strong spin-orbit interaction (SOI). Time reversal symmetry protects topological SS from backscattering in presence of weak perturbation [2–4]. This causes new possibility for practical applications particularly in realization of dissipationless spin transport which can be used in new spintronic devises.

A number of materials that hold non-trivial spin-polarized Dirac state has been intensively studied. Among them the Bi and Sb chalcogenides are most investigated TIs at present. Their band structure is widely studied [1, 5–10] and spin texture of the topological SS was observed both indirectly by use of circular dichroism [11] and directly by spin-resolved experiments [5, 12, 13]. However, besides the Dirac cone various types of SS states take place in TIs. Some of them can result in new physical phenomena. For example, angle-resolved photoemission spectroscopy (ARPES) measurements as well as time- and angle-resolved photoemission spectroscopy experiments [14] led to discovery of parabolic spin-split surface states in the principal energy gap just below the conduction band and M-shaped states in the local valence band gap [15–23].

Here, we study the conduction band (CB) energy gap surface states in the layered topological insulators Bi_2Se_3, $PbSb_2Te_4$, and $Pb_2Bi_2Te_2S_3$ by using density function theory (DFT) methods. The choice of these TIs is motivated by the fact they have different crystal structure, composed of quintuple (Bi_2Se_3), septuple ($PbSb_2Te_4$), and nonuple ($Pb_2Bi_2Te_2S_3$) layer blocks. Bi_2Se_3 is the extensively studied TI while $PbSb_2Te_4$ and $Pb_2Bi_2Te_2S_3$ were recently predicted as TIs [12, 24]. We show that except the Dirac cone in the principal gap and trivial unoccupied surface states a massless spin polarized surface state arises in the CB local gap at the $\bar{\Gamma}$. This state induced by the SOI inverted local gap has spin helicity similar to that of the Dirac state in the principal energy gap.

For electronic band calculations we employ two different computer codes that are based on DFT. The first one is the Vienna Ab Initio Simulation Package (VASP) [25, 26]. We used the generalized gradient approximation (GGA) [27] to the exchange correlation potential and the projector augmented wave (PAW) [28, 29] basis sets to solve the resulting Kohn–Sham system. The second approach used for electronic structure calculations is the full-potential linearized augmented plane-wave (FLAPW) method as implemented in the FLEUR code [30] with PBE for the exchange-correlation potential. The FLAPW basis has been extended by conventional local orbitals to treat quite shallow semi-core *d*-states. Both methods contained scalar relativistic corrections and spin-orbit coupling was taken into account

[1)] e-mail: eremeev@ispms.tsc.ru

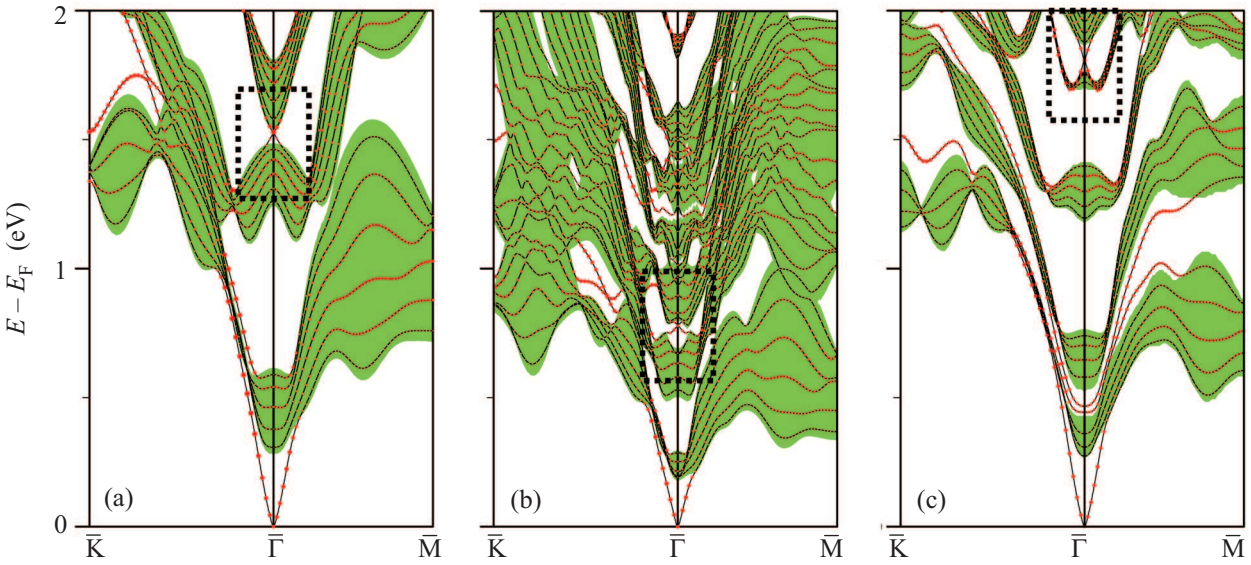

Fig. 1. (Color online) Surface electronic structure of Bi_2Se_3 (a), $PbSb_2Te_4$ (b), and $Pb_2Bi_2Te_2S_3$ (c) above E_F as calculated by VASP. Size of red circles correspond to the weight of the states in the outermost block. The projected bulk bands is shown in green. Dashed frames mark region of the unoccupied Dirac-like surface state

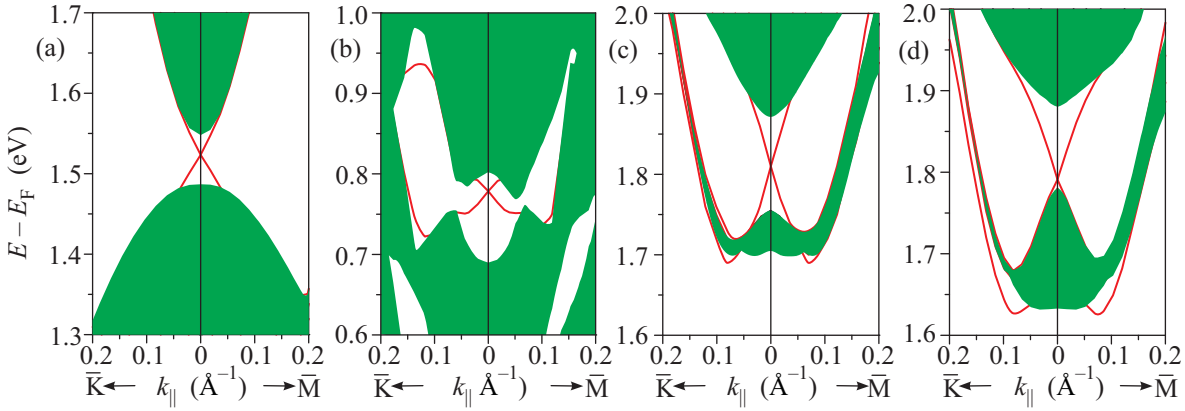

Fig. 2. (Color online) A magnified view of dashed frames marked in the Fig. 1 with CB cone in the center: (a) – Bi_2Se_3; (b) – $PbSb_2Te_4$; $Pb_2Bi_2Te_2S_3$ as calculated by VASP (c) and FLEUR (d) Codes

by the second variation method [31]. To simulate the (0001) surfaces of the TIs we use a slab composed of 6 quintuple layers (QLs) and 6 septuple layers (SLs) for Bi_2Se_3 and $PbSb_2Te_4$, respectively, and 5 nonuple layers (NLs) for $Pb_2Bi_2Te_2S_3$.

The calculated unoccupied electronic structure spectra in materials under interest is shown in Fig. 1. Shaded regions depict projected bulk bands onto the (0001) plane, while red dots indicate a weight of the states in the outermost structural block (QL, SL, NL). As easy to see in addition to the Dirac cone in the principal gap there exist different trivial surface states at the energies shown in Fig. 1 and at higher energies in the local CB gaps in all surfaces of interest.

At the same time in the conduction band energy gap there appears a Dirac-like surface state at the $\bar{\Gamma}$ point (framed in Figs. 1a–c by dashed line) for all compounds we study. In the case of Bi_2Se_3 this state arises at ~ 1.5 eV in gap of 70 meV formed by projection of the second and third bulk conduction bands. For $PbSb_2Te_4$ and $Pb_2Bi_2Te_2S_3$ the Dirac-like surface state takes place at ~ 0.8 and ~ 1.8 eV respectively. These states have the linear dispersion in the local gap and entering to the bulk states projection they transform into resonances and spread along the edges of the projection. A close-up of these states is shown in Fig. 2. Note that the Dirac-like surface state in the conduction band is well reproduced by both VASP and FLEUR calculations with some differences in the projected bulk bands (Figs. 2c and d).

In all considered TIs the unoccupied Dirac-like SS is isotropic with respect to $k_{||}$, i. e. the constant en-

ergy contours below and above the degeneracy point have an ideal circular shape as schematically shown in Fig. 3. The calculated orientation of the electron spin

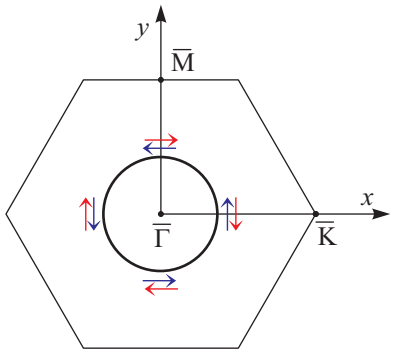

Fig. 3. (Color online) Schematic view of the spin structure of the CB cone. Red and blue arrows indicate spin direction for upper and lower part of the cone, respectively. Scales for constant energy contour and $2D$ Brillouin zone are different (typical maximal radius of the contour in materials under study is ~ 0.03 Å^{-1}; $\bar{\Gamma}$–$\bar{\mathrm{K}}$ direction is of ~ 1 Å^{-1})

within the surface state demonstrates in-plane spin polarization (out-of-plane component is negligibly small) with positive (clockwise) spin helicity in the upper part and negative helicity in the lower part of the Dirac cone, i. e. the same helicity as in the case of the topological SS located in the principal energy gap. Besides, owing to the SOI entanglement of the spin and orbital momenta the spin polarization in the CB cone is reduced and does not exceed 60% in Bi_2Se_3 and $Pb_2Bi_2Te_2S_3$ and is slightly smaller in $PbSb_2Te_4$ ($\sim 50\%$) that is comparable with the spin polarization in the conventional Dirac cone [32, 13].

In order to reveal the origin of formation of the second Dirac state in the conduction band of TIs consider first the bulk band structure of Bi_2Se_3. Note that a direct consequence of the inversion of the Bi and Se states in the principal gap at the Γ point in Bi_2Se_3 is formation of the Dirac cone in the principal energy gap. Let us consider the bulk conduction band of Bi_2Se_3 in the energy range of interest. Without spin-orbit coupling included the second and third conduction bands are degenerate along the Γ–Z direction (Fig. 4a). Spin-orbit interaction lifts this degeneracy and opens a gap between these bands at the Γ point (Fig. 4b). Thus, the gap supporting the new massless state in the conduction band results from the SOI. Both the upper and lower bands are mostly composed of the bismuth states, however, the Se p_z states of the central atomic layer of QL contribute to these bands too. As one can see in Fig. 4c, the weight of Se states in the lower band goes to zero approaching

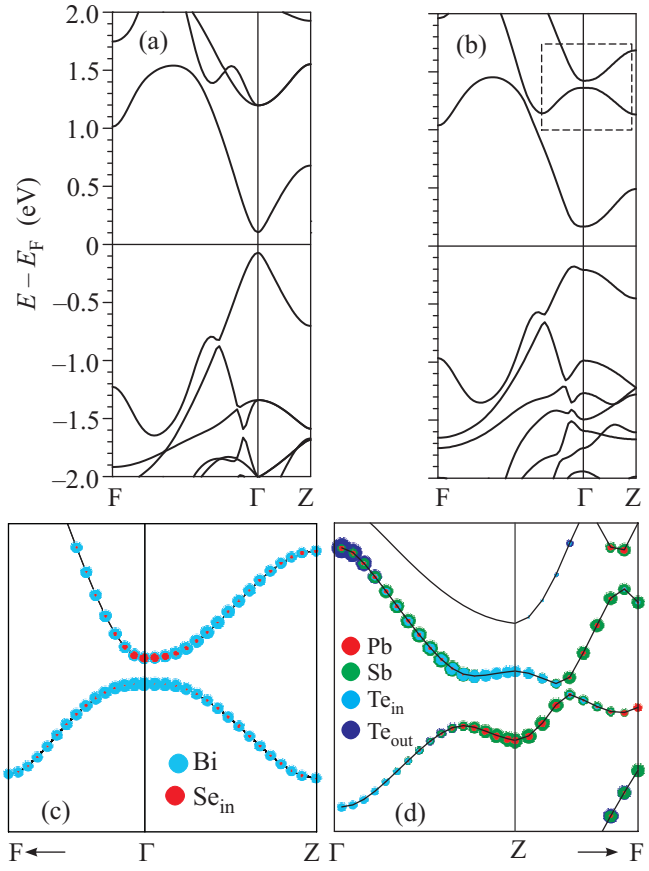

Fig. 4. (Color online) Bulk band structure of Bi_2Se_3 without (a) and with (b) SOI included. (c) – Magnified view of blue dashed frame marked in the Fig. 4b with composition of the second and third conduction bands in the vicinity of Γ. (d) – The same for $PbSb_2Te_4$ in the vicinity of Z

the Γ point. At the same time Se states in the upper band have maximal weight in the vicinity of Γ. Thus, this SOI-induced local gap at ~ 1.5 eV between the second and third conduction bands has inverted Se states. Like to the principal Γ gap where the states of the outer Se atoms of QL are inverted the states of the inner Se atom have a similar SOI-induced inversion in the CB gap. This fact points out that the CB Dirac cone is the unoccupied topological SS.

In the bulk band spectra of $PbSb_2Te_4$ the similar SOI-induced inversion can be detected for states of the inner Te atoms of SL in the vicinity of the Z point (Fig. 4d). However, in this ternary compound the picture is more complicated and it becomes even less obvious for quaternary TI $Pb_2Bi_2Te_2S_3$.

From this point of view it would be desirable to have such a simple technique to qualify unoccupied topological states as calculation of $\mathbb{Z}_2$ invariant. The difficulty is that the unoccupied cone is appeared in the local gap of

the bulk conduction band where along a path between time-reversal invariant momenta (TRIMs) in the Brillouin zone the gap in the spectrum of the bulk states closes and opens.

Analysis of the relation $(-1)^{\nu_0} = (-1)^{2P_3}$ [33] of the index ν_0 [2, 34] in the theory of topological insulators with the winding number $2P_3$ or with the non-Abelian Chern–Simons term in the k-space [35] using the continuous approach in the theory of topological invariants does not solve the problem. Thus we address the approach of Refs. [36–38] enabling us to determine the mechanism of reduction of the contribution made by bulk states to the topological invariant.

The origin of reduction of the contribution of the bulk states can be found by comparing the continuous and lattice versions of the $\mathbb{Z}_2$ invariant. It is shown in Ref. [36] that the $\mathbb{Z}_2$ invariant in the continuous case is expressed as

$$D = \frac{1}{2\pi i}\left[\oint_{\partial\mathcal{B}^-} A - \int_{\mathcal{B}^-} F\right] \mod 2, \qquad (1)$$

where $\mathcal{B}^- = [-\pi,\pi]\otimes[-\pi,0]$ is half of the Brillouin zone, $A = \mathrm{Tr}\,\psi^\dagger d\psi$ and $F = dA$ are the Berry gauge potential and the associated field strength respectively and $\psi(k)$ is the 2M(k)-dimensional ground state multiplet. The lattice analog of Eq. (1) is [37]

$$D_{\mathrm{L}} \equiv \frac{1}{2\pi i}\left[\sum_{k\in\partial\mathcal{B}^-} A(k) - \sum_{k\in\mathcal{B}^-} F(k)\right] = -\sum_{k\in\mathcal{B}^-} n(k) \mod 2, \qquad (2)$$

since $\sum_{k\in\mathcal{B}^-} F(k) = \sum_{k\in\partial\mathcal{B}^-} A(k) + 2\pi i \sum_{k\in\mathcal{B}^-} n(k)$. $n(k)$ in this equation are integers and $n(k) \bmod 2 \in \mathbb{Z}_2$ due to the residual $U(1)$ invariance [37]. From Eq. (2) we can conclude that the reason for cancelation of the bulk continuum states is the compactness of the lattice gauge theory. In all TIs under study at energy of CB Dirac state there are gaps in Γ, F_i, L_i, and Z TRIMs in the case of rhombohedral Bi_2Se_3 and $PbSb_2Te_4$ or in Γ, M_i, L_i, and A TRIMs of hexagonal $Pb_2Bi_2Te_2S_3$ which allow us to implement the parity analysis [34] to calculate the topological number ν_0 for the CB cone in these systems by fixing of an isoenergy level in the local gap, supporting the unoccupied Dirac cone.

The results for $PbSb_2Te_4$ show that non-trivial value $\nu_0 = 1$ of the topological invariant for the unoccupied cone is provided by the change of the parity at the Z point (where we have revealed the inversion of $\mathrm{Te}_{\mathrm{in}}$ states, see Fig. 4d). In the case of $Pb_2Bi_2Te_2S_3$ the change of parity in the A point in the gap between 4-th and 5-th bulk conduction bands determines topologically non-trivial ν_0 and the appearance of the unoccupied Dirac cone in the surface electronic spectrum. Thus inversion of the local gap edges in the conduction band along with the presence of non-inverted gaps in other TRIMs of the bulk Brillouin zone at the same energy is responsible for the emergence of single Dirac-like helical spin surface state in the topological insulators.

In summary, we have examined the unoccupied electronic spectra of the layered topological insulators with different composition and crystal structure. We revealed that except for trivial conduction band surface states a massless topologically-protected helical spin state exists in the narrow local conduction band gap at the $\bar{\Gamma}$ point in all materials under study. This state arises owing to inversion of the certain bulk conduction bands at the time-reversal invariance momentum points Γ, Z, and A of Bi_2Se_3, $PbSb_2Te_4$, and $Pb_2Bi_2Te_2S_3$, respectively. The observed state has the same spin helicity as in the conventional Dirac cone in the principal energy gap. The revealed CB topological states provide a pathway to the measurements on excitations between two Dirac spin polarized states at the surface of layered topological insulators.

This work was supported by grant of Government of the Russian Federation regulation 220, contract # 11.G34.31.0028 (November 25, 2010).

1. H. Zhang, C.-X. Liu, X.-L. Qi et al., Nature Phys. **5**, 438 (2009).
2. L. Fu, C. L. Kane, and E. J. Mele, Phys. Rev. Lett. **98**, 106803 (2007).
3. X.-L. Qi, T. L. Hughes, and S.-C. Zhang, Phys. Rev. B **78**, 195424 (2008).
4. P. Roushan, J. Seo, C. V. Parker et al., Nature **460**, 1106 (2009).
5. D. Hsieh, Y. Xia, D. Qian et al., Nature **460**, 1101 (2009).
6. Y. L. Chen, J. G. Analytis, J.-H. Chu et al., Science **325**, 178 (2009).
7. T. Zhang, P. Cheng, X. Chen et al., Phys. Rev. Lett. **103**, 266803 (2009).
8. K. Kuroda, M. Arita, K. Miyamoto et al., Phys. Rev. Lett. **105**, 076802 (2010).
9. S. Xu, L. Wray, T. Xia et al., arXiv:1007.5111.
10. S. V. Eremeev, Yu. M. Koroteev, and E. V. Chulkov, Pis'ma v ZhETF **91**, 419 (2010) [JETP Lett. **91**, 387 (2010)].
11. Y. H. Wang, D. Hsieh, D. Pilon et al., Phys. Rev. Lett. **107**, 207602 (2011).
12. S. V. Eremeev, G. Landolt, T. V. Menshchikova et al., Nature Commun. **3**, 635 (2012).

13. K. Miyamoto, A. Kimura, T. Okuda et al., Phys. Rev. Lett. **109**, 166802 (2012).
14. J. A. Sobota, S. Yang, J. G. Analytis et al., Phys. Rev. Lett. **108**, 117403 (2012).
15. M. Bianchi, D. Guan, S. Bao et al., Nature Comm. **1**, 128 (2010).
16. L. A. Wray, S.-Y. Xu, Y. Xia et al., Nature Phys. **7**, 32 (2011).
17. Z.-H. Zhu, G. Levy, B. Ludbrook et al., Phys. Rev. Lett. **107**, 186405 (2011).
18. T. V. Menshchikova, S. V. Eremeev, and E. V. Chulkov, Pis'ma v ZhETF **94**, 110 (2011) [JETP Lett. **94**, 106 (2011)].
19. L. A. Wray, S. Xu, M. Neupane et al., arXiv:1105.4794v1
20. T. Valla, Z.-H. Pan, D. Gardner et al., Phys. Rev. Lett. **108**, 117601 (2012).
21. M. G. Vergniory, T. V. Menshchikova, S. V. Eremeev et al., Pis'ma v ZhETF **95**, 230 (2012) [JETP Lett. **95**, 213 (2012)].
22. S. V. Eremeev, M. G. Vergniory, T.V̇. Menshchikova et al., New Journal Physics, will be published in November (2012).
23. H. M. Benia, C. Lin, K. Kern et al., Phys. Rev. Lett. **107**, 177602 (2011).
24. I. V. Silkin, T. V. Menshchikova, M. M. Otrokov et al., Pis'ma v ZhETF **96**, 352 (2012) [JETP Lett. **96**, 322 (2012)].
25. G. Kresse and J. Hafner, Phys. Rev. B **48**, 13115 (1993).
26. G. Kresse and J. Furthmüller, Comput. Mater. Sci. **6**, 15 (1996).
27. J. P. Perdew, K. Burke, and M. Ernzerhof, Phys. Rev. Lett. **77**, 3865 (1996).
28. P. E. Blöchl, Phys. Rev. B **50**, 17953 (1994).
29. G. Kresse and D. Joubert, Phys. Rev. B **59**, 1758 (1999).
30. http://www.flapw.de.
31. D. D. Koelling and B. N. Harmon, J. Phys. C **10**, 3107 (1977).
32. O. V. Yazyev, J. E. Moore, and S. G. Louie, Phys. Rev. Lett. **105**, 266806 (2010).
33. Z. Wang, X.-L. Qi, and S.-C. Zhang, New J. Phys. **12**, 065007 (2010).
34. L. Fu and C. L. Kane, Phys. Rev. B **76**, 045302 (2007).
35. X.-L. Qi, T. Hughes, and S.-C. Zhang, Phys. Rev. B **78**, 195424 (2008).
36. L. Fu and C. L. Kane, Phys. Rev. B **74**, 195312 (2006).
37. T. Fukui and Y. Hatsugai, J. Phys. Soc. Jpn. **76**, 053702 (2007).
38. See also the analysis of the paper N.A. Usov, Sov. Phys. JETP **67**, 2565 (1988) for time inversal symmetry breaking systems.